Seismic Behavior of Post-Tensioned Self-Centering Precast Concrete Dual-Shell Steel Columns

Gabriele Guerrini S.M.ASCE[1], José I. Restrepo M.ASCE[2], Milena Massari[3], Athanassios Vervelidis[4]

ABSTRACT

This paper describes an innovative bridge column technology for application in seismic regions. The proposed technology combines a precast post-tensioned composite steel-concrete hollow-core column, with supplemental energy dissipation, in a way to minimize post-earthquake residual lateral displacements. The column consists of two steel cylindrical shells, with high-performance concrete cast in between. Both shells act as permanent formwork; the outer shell substitutes the longitudinal and transverse reinforcement, as it works in composite action with the concrete, whereas the inner shell removes unnecessary concrete volume from the column, prevents concrete implosion, and prevents buckling of energy dissipating dowels when embedded in the concrete. Large inelastic rotations can be accommodated at the end joints with minimal structural damage, since gaps are allowed to open at these locations and to close upon load reversal. Longitudinal post-tensioned high-strength steel threaded bars, designed to respond elastically, in combination with gravity forces ensure self-centering behavior. Internal or external steel devices provide energy dissipation by axial yielding. This paper describes the main requirements for the design of these columns, and also discusses the experimental findings from two quasi-static tests.

[1] Ph.D. Candidate, Dept. of Structural Engineering, University of California at San Diego
9500 Gilman Dr., MC 0085, La Jolla, CA 92093-0085, USA. Email: gguerrin@ucsd.edu

[2] Professor, Dept. of Structural Engineering, University of California at San Diego
9500 Gilman Dr., MC 0085, La Jolla, CA 92093-0085, USA. Email: jrestrepo@ucsd.edu

[3] Civil Engineer, Patricio Bonelli and Associates
Av. Libertad 269, Oficina 905, Viña del Mar, Chile. Email: massari.milena@libero.it

[4] Civil Engineer
V. Vagna 48, Bussi sul Trino (PE), 65022, Italy. Email: atverve@live.it

KEYWORDS: Bridge column; Composite column; Energy dissipation; Hybrid rocking; Post-tensioning; Seismic design; Self-centering; Testing.

INTRODUCTION

Current provisions for seismic design of bridges (Caltrans, 2010; AASHTO, 2012) allow columns to respond beyond the elastic limit under the design earthquake, and to be damaged provided that collapse is prevented. Inelastic behavior is localized within flexural plastic-hinge regions at the bottom and/or top of the columns. These regions may experience some structural damage during the design-level earthquake and such damage may lead to temporary closure of the bridge to the public. However, the consequences of structural damage in a bridge system can be critical if associated with the interruption of an important road path: obstruction of rescue and recovery operations, and economical losses related to business interruption and displacement of people and goods (Palermo et al., 2008).

While the concept of structural damage is widely accepted in design, resilient communities expect strategic structures and bridges to survive moderately strong earthquakes with little or no disturbance to traffic and business. In other words, partial or total bridge closures are tolerated with uneasiness, particularly in heavily congested urban areas. As a consequence, research efforts have been aligned at developing bridge technologies that minimize structural damage, to encompass self-centering properties (Restrepo et al., 2011; Guerrini et al., 2011), and to reduce construction time and traffic impact (FHWA, 2012; Culmo, 2011).

This paper describes the main findings of an experimental work on two post-tensioned self-centering precast concrete dual-shell steel columns, and describes the design criteria. The work presented here is an enhancement to the earlier research described in Restrepo et al. (2011).

BACKGROUND

Self-Centering/Rocking Systems

The concept of hybrid self-centering structural behavior originated from the features incorporated in the design of the "stepping" railway bridge over the South Rangitikei River, New Zealand (Cormack, 1988) commissioned in 1981, where rocking is combined with a hysteretic energy dissipation device. Similar features were provided to an industrial chimney of the Christchurch, New Zealand airport (Sharpe and Skinner, 1983). The idea was then applied to moment-frame and coupled-wall buildings, chiefly under the *PREcast Seismic Structural Systems* (PRESSS) program (Priestley and Tao ,1993; MacRae and Priestley, 1994; Stone et al. ,1995; El-Sheikh et al., 1999; Kurama et al. 1999,Nakaki et al., 1999; Priestley et al., 1999). Christopoulos et al. (2002) extended the concept to steel moment frames. Additional experimental work on self-centering structural walls was also reported by Pérez et al. (2003), Holden et al. (2003), Restrepo and Rahman (2007), and Toranzo et al. (2009).

Apart from the South Rangitikei River bridge, the early development of hybrid systems was mainly focused on implementation in buildings; however, interest in the use of rocking systems in bridges increased in the past fifteen years. One of the pioneering experimental studies on the use of rocking bridge columns incorporating unbonded post-tensioning was carried out by Mander and Cheng (1997). This project was followed by an experimental program conducted by Hewes and Priestley (2002) in which the response of segmental bridge piers incorporating unbonded post-tensioning was investigated. A number of analytical studies were subsequently carried out considering potential applications of self-centering solutions to bridge columns (Kwan et al., 2003; Kwan et al., 2003; Sakai et al., 2004; Palermo et al., 2005; Heiber et al., 2005; Ou et al., 2006; Palermo et al. 2008). Shake table testing of cast-in-place hybrid concrete bridge columns was performed by Sakai et al.(2006). Palermo et al. (2007) and Marriott et al. (2009, 2011) carried out analytical studies and quasi-static cyclic tests on monolithic, purely rocking ,and hybrid concrete columns, developing different solutions for energy dissipation. Solberg et al. (2009) conducted quasi-static and pseudo-dynamic bidirectional tests on hybrid post-tensioned bridge columns with armored rocking interfaces. Ou et al. (2010) performed large-scale experiments on precast segmental post-tensioned bridge columns.

Concrete-Filled Tube (CFT) Columns

Concrete-filled tubes (CFT), also termed steel sections filled with concrete or filled composite sections, are a type of composite steel-concrete columns which has gained interest for seismic applications in the past three decades (Shanmugam et al., 2001). Tests conducted by Ghosh (1977) demonstrated the beneficial effect of concrete filling on the load and moment carrying capacity. Experiments on circular CFT columns were conducted by Prion et al. (1989) to study the effect of concrete confinement. Shakir-Khalil and Zeghiche (1989) and Shakir-Khalil and Mouli (1990) tested the strength and failure modes of rectangular in-filled composite columns under axial load and bending, including the use of high strength concrete. Ge and Usami (1992) studied local buckling modes of stiffened and unstiffened in-filled columns. Rangan and Joyce (1992), O'Brien and Rangan (1993), and O'Shea and Bridge (1995) tested eccentrically loaded slender steel tubular columns filled with high-strength concrete, while Uy and Patil (1996) studied the behavior of concrete-filled high-strength steel fabricated box columns. Virdi and Dowling (1973) investigated the bond between concrete and steel tube; mechanical connectors are necessary for transferring shear between concrete and steel tube when bond capacity is likely to be exceeded (Gebman et al. 2006). Suzuki and Kato (1981) observed that in relatively short CFTs, the confined concrete can act as a diagonal compression strut together with tension field action of the steel side walls. A number of analytical methods for the calculation of the ultimate strength of CFT columns have been proposed by Knowles and Park (1969), Neogi et al. (1969), Rangan and Joyce (1992), Ge and Usami (1994), Bradford (1996), Kato (1996), Wang and Moore (1997), Leon et al. (2007).

Sakino and Tomii (1981) and Sakino and Ishibashi (1985) examined the behavior of short- and intermediate-length square CFT columns, subjected to cyclic lateral forces with constant axial load. Park et al. (1983) performed an experimental and theoretical investigation into the seismic behavior of steel-encased circular reinforced concrete bridge piles. Boyd et al. (1995) and Itani (1996) studied the ductility and energy dissipating capacity of columns with studded and non-studded steel shells. Kitada

(1998) studied the difference in local buckling modes between cross-sections of steel and composite columns in bridge columns and buildings; in particular, he observed that the ductility of the composite beam-column specimen with rectangular cross-section is smaller compared to that with a circular cross-section in the case of large axial compression. In fact, as noticed by Matsui et al. (1995), circular tubes provide a significant amount of confinement, while this effect is negligible in the case of rectangular tubes as the hoop tension developed along the side walls is not constant.

SYSTEM DESCRIPTION

The bridge column described herein consists of two concentric cylindrical steel shells (*dual-shell* technology) running for its entire height. High-performance concrete with high strength, high slump, and reduced shrinkage is sandwiched in between the shells and longitudinal reinforcement is detailed only between the column ends and the footing or bent cap (see Fig. 1(*a*)). The outer shell acts as permanent formwork, providing also longitudinal and transverse reinforcement, as it works in composite action with the concrete. The inner shell provides permanent formwork too, reducing unnecessary weight and making the technology suitable for prefabrication and rapid erection. It also prevents concrete implosion upon crushing under large compressive strains, which may develop upon gap opening, and delays buckling of energy dissipating dowels which are embedded in the concrete.

Large inelastic rotations can be sustained at the column-footing and column-cap beam joints with minimal structural damage. These rotations are accommodated within the connections themselves, through the formation of gaps at the member interfaces (Fig. 1(*b*)): gaps are allowed to open in tension under severe lateral displacement demand, and to practically close at the end of the excitation. Self-centering/rocking capability is provided by gravity forces and unbonded, threaded post-tensioning (PT) bars, designed to remain elastic. The bolted PT bar anchorages at the bent cap and foundation allow for eventual bar replacement, should corrosion or other types of damage be a concern.

Energy dissipation takes place through axial yielding of internal dowels (Restrepo and Rahman, 2007; Restrepo et al., 2011), as shown in Figure 1(*b*), or external devices (Cormack, 1998; Marriott et al., 2009; Toranzo et al., 2009), preventing the main structural members from experiencing significant damage. Under strong-intensity earthquake excitation only these devices may undergo multiple cycles within the inelastic range, with possible need of replacement, but the structure is expected to remain functional overall. To transfer tension between the internal dowels and the outer shell, circumferential weld beads are provided on the internal surface of the outer shell, only near its ends (Gebman et al., 2006; Restrepo et al., 2011). External dissipators are simply welded to brackets preinstalled on the outer shell and onto the footing or bent cap.

PERFORMANCE OBJECTIVES AND DESIGN CRITERIA

Columns of this type can be easily designed for a single performance level, say the design-basis earthquake. Seven criteria should be met to ensure satisfactory performance of the proposed column technology for this performance level: (i) minimum outer shell thickness, (ii) energy dissipation force capacity, (iii) composite action, (iv) mortar bed integrity, (v) concrete strain control, dowel buckling, and inner shell diameter, (vi) prevention of early dissipator fracture, and (vii) prevention of early loss of post-tensioning force. These seven criteria are described below in more detail.

Criterion (i): Minimum Outer Shell Thickness

As the external shell provides confinement to the compressed concrete, tensile hoop strains arise in the shell. When the column is subjected to the target lateral displacement, these strains should be kept below the yield strain, to avoid permanent deformation and damage to the shell and to preserve the composite action with the encased concrete. To meet this objective, based on previous experiments (Gebman et al., 2006; Restrepo et al., 2011) and the tests reported here, outer shell diameter to thickness ratios should be $D_O / t_O \leq 100$. Such ratio results in a minimum volumetric confinement ratio for the concrete of 4% calculated over the solid volume of the column, which adequately confines the high-strength concrete recommended for this application. In addition, the shell should possess sufficient strength to ensure that the flexural strength of the composite column, at the section where the dowel bars end or where the external energy dissipators are welded to the shell, is equal or greater than that required by capacity design, assuming that flexural overtstrength develops at the column end or ends where joint opening will take place. However, this last condition is not expected to control the design.

Criterion (ii): Energy Dissipation Force Capacity

Recentering forces, provided by gravity and post-tensioning, and energy dissipating forces need to be well balanced, to obtain the desired self-centering response and sufficient energy dissipation. Gravity and post-tensioning forces must be large enough to overcome the overstrength capacity of the energy dissipators, thus forcing them to yield in compression and to close the gap at each load reversal (Restrepo and Rahman, 2007); that is:

$$\Lambda_C = \frac{F_{ED,u}^{(t)}}{P_u + F_{PT,e}^{(t)}} \leq 0.6 \tag{1}$$

where P_u is the design gravity force, $F_{PT,e}^{(t)}$ is the total effective post-tensioning force (after time-dependent losses), $F_{ED,u}^{(t)}$ is the total ultimate strength of all energy dissipators, and Λ_C is a recentering coefficient. The limitation on Λ_C could be theoretically be made equal to 1.0 (i.e. equality between dissipators overstrength force and recentering forces), but a limit of 0.6 is suggested to account for uncertainties on post-tensioning losses and, primarily, for the presence of debris upon gap opening in the rocking interfaces.

In parallel, enough energy dissipation should be provided to the system, to avoid the large scatter on lateral displacement demands observed on purely rocking systems (Makris et al. 1998). For this reason, a second condition should be satisfied:

$$\Lambda_D = \frac{F_{ED,u}^{(t)}}{P_u + F_{PT,e}^{(t)} + F_{ED,u}^{(t)}} \geq 0.1 \tag{2}$$

where Λ_D is an energy dissipation coefficient.

Criterion (iii): Composite Action

If internal dowels are used for energy dissipation, tensile stresses need to be transferred from the dowels to the outer shell, in order to develop composite steel-concrete action. As friction between steel and concrete cannot be relied on, mechanical connectors are needed: for this purpose, circumferential weld beads or bars welded on the internal surface of the outer shell can be provided along the development length of the dowels (Gebman et al., 2006; Restrepo et al., 2011). Weld beads having a size similar to the outer shell thickness, spaced at about 10 times their size, proved to be sufficient to develop the stress transfer and ensure composite action (Gebman et al., 2006).

Criterion (iv): Mortar Bed Integrity

Under the design-basis earthquake, crushing of the mortar layer between column and footing or column and cap beam should be avoided, as it can lead to post-tensioning losses. The integrity of the mortar could be ensured by checking that, at the smeared curvature corresponding to the joint opening under the target lateral displacement, the neutral axis depth ratio to the column diameter is less than c/D_O = 0.25. For design purposes, it can be assumed that upon gap opening the extreme compressive fiber shortens by $\theta_j c$ (Restrepo and Rahman, 2007), where θ_j is the target joint rotation; this means that the extreme mortar compressive strain is taken equal to the joint rotation. Given the joint rotation and the yield-segment length of the energy dissipators, L_{YED} (see Criterion (vi)), the forces on the dissipators can be calculated; then conventional reinforced-concrete section equilibrium methods can be applied to determine the neutral axis depth. The upper-bound c/D_O = 0.25 is suggested to limit the area of mortar subjected to large compressive strain demand and to retain enough stiffness.

Criterion (v): Concrete Strain Control, Dowel Buckling, and Inner Shell Diameter

In practical applications, a readily available lock-seam, helical corrugated steel pipe conforming to ASTM A760 (2010) can be used as the inner shell. To prevent significant inner shell plastic deformations due to column concrete dilation, the neutral axis under the design-basis lateral displacement should not cut the hollow core, even though a compressive strain of 0.1% can be tolerated on the column concrete at the inner circle; this limitation defines the maximum diameter allowed for the inner shell. The neutral axis depth and the concrete strain at the inner circle can be determined as for Criterion (iv). Strength and stiffness of the thinnest commercially available corrugated drainage pipes are expected to be sufficient to prevent inward buckling of embedded energy dissipating dowels.

Criterion (vi): Prevention of Early Dissipator Fracture

Gap opening will induce significant elongation on the energy dissipators. Internal or external steel devices have to yield along a specific segment L_{YED} to accommodate this elongation, without fracturing under the design-basis lateral displacement. To prevent low-cycle fatigue fracture, the strain along the yield segment should be limited to half the value $\varepsilon_{ED,u}$ corresponding to the peak tensile stress. For a joint rotation θ_j, the required yield segment length L_{YED} is given by:

$$L_{YED} = \frac{2 \cdot \left[\theta_j \cdot \left(d_{ED}^{(e)} - c\right) - \Lambda_S \cdot 12 \cdot \varepsilon_{ED,y} \cdot d_{b,ED}\right]}{\varepsilon_{ED,u}} \tag{3}$$

where $d_{ED}^{(e)}$ is the distance of the extreme tensile dissipator from the extreme compressive fiber, $\varepsilon_{ED,y}$ is the yield strain of the dissipator steel, $d_{b,ED}$ is the diameter of the energy dissipating bar (the reduced diameter for milled bars), and c is the neutral axis depth at the design-basis lateral displacement demand, which can be determined as for Criterion (iv). The second term at the numerator of Eq. 3 accounts for yield strain penetration along the development length of non-milled energy dissipators embedded in concrete, which is assumed to be 6 bar diameters at each end (Park and Paulay, 1990). Λ_S is a strain-penetration coefficient: $\Lambda_S = 1$ for non-milled debonded bars, in which strain penetration out of the yield segment occurs; $\Lambda_S = 0$ for dog-bone milled bars, where strain penetration is prevented. For design purposes, it is conservative to determine the required yield segment length by assuming c = 0 and $\Lambda_S = 0$ in Eq. (3); moreover, the joint rotation θ_j at the design earthquake can be made equal to the column drift ratio, thus, ignoring the elastic flexibility of the dual-shell column.

Criterion (vii): Prevention of Early Loss of Post-Tensioning Force

When the gap opens at the column-footing and/or column-cap interface, the post-tensioning bars will elongate as Figure 1(*c*) shows. If any of the PT bars yields, that bar will display a permanent plastic elongation when the gap closes, causing a loss of post-tensioning force and compromising the self-centering ability. To delay these bars from yielding at the design-basis earthquake, additional deformability can be added to each PT bar by placing elastic devices in series with the bars to add flexibility. Elastomeric bearing pads, inserted between the top anchor plate and the cap beam, have proved to be satisfactory for this scope. With this configuration the tensile deformation demand on the bars is partially transformed into compressive deformation of the bearing pads.

If $F_{PT,e}^{(b)}$ and $F_{PT,y}^{(b)}$ are the effective (after time-dependent losses) and yield post-tensioning force on the extreme tensile bar *b*, located at $d_{PT}^{(b)}$ from the extreme compressive fiber, the yield condition under a joint rotation θ_j at n_j column end joints ($n_j = 1$ for cantilever, $n_j = 2$ for fixed-fixed columns) is given by:

$$F_{PT,y}^{(b)} = F_{PT,e}^{(b)} + \frac{n_j \cdot \theta_j \cdot \left(d_{PT}^{(b)} - c\right)}{\dfrac{L_{UPT}}{E_{PT} \cdot A_{PT}^{(b)}} + \dfrac{1}{K_B^{(b)}}} \tag{4}$$

where *c* is the neutral axis depth from the extreme compressive fiber; L_{UPT}, E_{PT}, and $A_{PT}^{(b)}$ are the unbounded length, the elastic modulus, and the cross-sectional area of PT bar *b*; and $K_B^{(b)}$ is the stiffness of the bearing or other deformable device in series with bar *b*.

For a design-basis total joint rotation $\theta_j^* = n_j \cdot \theta_j$ (sum of the top and bottom joint rotations) the required bearing-to-bar stiffness ratio can be found from Eq. 4 as:

$$\frac{K_B^{(b)}}{K_{PT}^{(b)}} = \frac{1}{n_j \cdot \theta_j \cdot \dfrac{d_{PT}^{(b)} - c}{\left(\varepsilon_{PT,y}^{(b)} - \varepsilon_{PT,e}^{(b)}\right) \cdot L_{UPT}} - 1} = \frac{1}{\theta_j^* \cdot \Lambda_B - 1} \tag{5}$$

where $K_{PT}^{(b)} = E_{PT} A_{PT}^{(b)} / L_{UPT}$ is the axial stiffness of PT bar *b*; $\varepsilon_{PT,e}^{(b)}$ and $\varepsilon_{PT,y}^{(b)}$ are the strains on bar *b* due to the effective post-tensioning and yield forces; and

$$\Lambda_B = \frac{d_{PT}^{(b)} - c}{\left(\varepsilon_{PT,y}^{(b)} - \varepsilon_{PT,e}^{(b)}\right) \cdot L_{UPT}} \tag{6}$$

where Λ_B is a non-dimensional coefficient. Smaller values of Λ_B denote systems less sensitive to PT bar yielding.

For design purposes, the joint rotation θ_j can be approximated by the corresponding drift-ratio. If Eq. 5 gives a negative value, no bearing is required. Furthermore, a positive value larger than 10 calculated from Eq. 5 indicates that the bearing pad would be very stiff compared to the bar, and would accommodate very small deformations, thus providing negligible additional flexibility.

A design chart derived from Eq. 5 is plotted on Figure 2. It can be observed that, for large total joint rotations, very flexible bearings are required (low required stiffness ratios), and their stiffness is quite insensitive to the rotation demand. However, because of the inverse proportionality relationship between the stiffness ratio and the total joint rotation, when θ_j^* decreases the need of bearings becomes suddenly negligible (high required stiffness ratios), as the curves become very steep. The threshold between these two regions depends on the coefficient Λ_B; it can be noted that the bearings become completely ineffective (required stiffness ratio going to infinity) when $\theta_j^* = 1/\Lambda_B$.

The force-deformation characteristics of some elastomers, being Voigt materials, can be sensitive to the loading rate. The bearing stiffness $K_B^{(b)}$ should then be based on the material properties at a loading rate comparable to the real one under seismic excitation. This rate can be estimated dividing the range $F_{PT,y}^{(b)} - F_{PT,e}^{(b)}$ by one quarter of the structure's fundamental period.

Creep properties of the elastomeric material should be accurately known and accounted for, as time-dependent deformations of the bearings may affect significantly the long-term magnitude of the post-tensioning force. Post-tensioning losses in the order of 20% to 40% of the initial force (after lock-off losses) may be anticipated, depending on the applied force, on the area and thickness of the bearing, and on the length of the PT bar. Incremental post-tensioning can help reducing the amount of losses due to bearing creep: most of the creep deformation happens during the first few hours after loading, and can be partially compensated by staged post-tensioning.

TEST SPECIMENS

Target Performance Objectives

Two column test units were designed for a target drift ratio of 3% without structural damage. At this drift ratio, post-tensioning bars were expected to remain elastic, and the stiffness of the elastomeric bearings was determined accordingly. Also, the energy dissipators were designed not to fracture at the target drift ratio: the milled length of the external buckling-restrained devices and the debonded length of the internal dowels were calculated on this basis. In order to preserve the system self-centering behavior at the target drift ratio, the mortar bed was designed to crush under larger lateral displacements.

Test Specimens Details and Materials

Two *dual-shell* cantilever bridge column units were tested at the UC San Diego Powell Structural Engineering Laboratories (Fig. 3): Unit 1A was equipped with external buckling-restrained energy dissipators, while Unit 1B incorporated internal dowel bars (see Figures 4, 5, and 6). The test units were built at 1 to 2.4 scale. Given their precast nature, footing, column, and load stub were cast separately; after concrete had hardened, they were initially assembled as Unit 1A. When testing of Unit 1A was completed, the three components were taken apart, the column was flipped upside-down, and they were reassembled as Unit 1B. In fact, only the bottom region of the column was subjected to large strains and minor damage during the first test, while the other end was still free of any damage. By doing this, it was possible to take advantage of both ends of the element.

The overall column diameter was 0.51 m (20 in.), its height was 0.84 m (33 in.), and the total cantilever span from the base to the point of lateral load application was 1.13 m (44.5 in.). A low aspect ratio of 2.2 was chosen to subject the specimens to more critical conditions of shear sliding at the base. Moreover, a short element can accommodate short post-tensioning bars, which are more susceptible to yielding due to their lower axial deformability.

The column outer shell had a diameter D_O = 0.51 m (20 in.) and a thickness t_O = 6.4 mm (0.25 in.), that is D_O / t_O = 80. The inner shell had a diameter D_I = 0.36 m (14 in.) and a thickness t_I = 3.2 mm (0.125 in.), that is D_I / t_I = 112. Details are shown in Figure 4. The shells were obtained by folding and welding plates made of Grade 50 A572 steel. In practice, the inner shell would be a corrugated drainage pipe (Restrepo et al., 2011). High-performance, normal-weight concrete was used to cast column, footing, and load stub, with a specified compressive strength of 62 MPa (9.0 ksi) at 56 days. The compressive strengths measured at 28 days, 49 days (day of testing of Unit 1A) and 96 days (day of testing of Unit 1B) were 66 MPa (9.5 ksi), 70 MPa (10.2 ksi), and 72 MPa (10.4 ksi), respectively. The outer shell was equipped with six radially distributed 12.7-mm (0.5-in.) thick steel brackets, welded to the external surface (Fig. 4(*a*)), for the connection of the buckling-restrained dissipators of Unit 1A. Six 50.8-mm (2-in.) diameter, 0.46-m (18-in) long, corrugated metal ducts were embedded in the concrete for the installation of the internal dowels of Unit 1B (Fig. 4(*b*)); three circumferential 9.5-mm (3/8-in.) weld beads on the internal surface of the outer shell provided tensile stress transfer between the dowels and the shell (Fig. 6(*c*)).

A 12.7-mm (0.5-in.) thick mortar bed was cast at the column-to-footing connection, to compensate for expected in-situ construction tolerances. A high-performance metallic grout mix placed at plastic consistency in the form of a mortar bed was used in Unit 1A. The mortar compressive strengths were 46.4 MPa (6.7 ksi) and 49.2 MPa (7.1 ksi) at 29 and 49 days (day of testing of Unit 1A), respectively. For the column-footing joint of Unit 1B the same product was used, but polypropylene fibers were added in the proportion of 0.035% by weight to increase the mortar toughness; strengths of 53.4 MPa

(7.8 ksi) and 52.9 MPa (7.7 ksi) were obtained at 28 and 35 days (day of testing Unit 1B). The mortar was scraped from underneath the outer shell, to prevent the shell from causing premature crushing under direct compression transfer, a problem noted in earlier experiments (Restrepo et al., 2011).. Since the upper joint between column and load stub was not critical because of the low bending moment at this location, hydrostone was placed to match the two pieces there. All interface surfaces were roughened to improve shear-friction transfer. A bond-breaker film was applied to the bottom surface of the column, to allow separation from the mortar bed and opening of the gap.

Six external, buckling-restrained, energy dissipators were incorporated in test Unit 1A, radially distributed around the column perimeter (Fig. 5). These devices consisted of steel bars with a reduced diameter over a specific length, where dissipation was provided by material hysteresis. Each 343-mm (13.5-in.) long steel bar had an original diameter of 25.4 mm (1 in.), which was reduced to 14.3 mm (9/16 in.) in the 165-mm (6.5-in.) long milled portion. Hot-rolled Grade 1018 A576 steel was used, with a measured yield strength of 331 MPa (48 ksi), ultimate tensile strength of 490 MPa (71 ksi), and strain of 23% at the ultimate tensile strength. In order to prevent buckling, the milled part was encased and grouted within a steel pipe; grease was used to reduce friction between bar and grout. Mastic tape, about 3-mm (0.125-in.) thick, was applied along the tapered segments, to minimize bearing of the non-milled ends on the filling grout. The external dissipators were welded to anchors within the footing and to the column outer-shell brackets.

Unit 1B was equipped with six internal dowels at the column-footing joint, acting as internal energy dissipators (Fig. 6). Grade 75 316LN stainless steel #4 deformed bars were used for this purpose. The bars were wrapped with duct-tape for a length of 178 mm (7 in.) across the column-footing interface to inhibit the bond within this length. Material testing showed a yield stress for the stainless steel bars of 745 MPa (108 ksi), an ultimate tensile strength of 889 MPa (129 ksi), and a strain of 22% at the ultimate tensile strength. The dowels were first grouted within corrugated steel ducts predisposed in the footing, then, after column placement on the footing, they were grouted within the column ducts. The footing grout had a compressive strength of 52.7 MPa (7.6 ksi) on the day of testing, while the column grout showed a compressive strength of 59.2 MPa (8.6 ksi).

Four 34.9-mm (1-3/8 in.) diameter, A722 Grade 150 threaded bars provided the post-tensioning force to both units. The total effective post-tensioning force was 845 kN (190 kips) in Unit 1A and 890 kN (200 kips) in Unit 1B, after all losses. Jacking forces of 311 kN (70 kips) were applied to each bar, to compensate for lock-off and bearing creep losses. The bars ran within the column hollow core, sleeved in ducts filled with fluid grout to simulate corrosion protection and were screwed into anchorage devices prearranged in the footing, allowing for bar replacement. Additional bar deformability was provided by placing in series with the post-tensioning bars rubber (Unit 1A) or polyurethane (Unit 1B) bearings, between the top anchorage plates and the load stub.

A bearing consisting of five square 80-Shore-A hardness rubber pads was provided to each post-tensioning bar in test Unit 1A. The pads were 190.5 mm (7.5 in.) square by 25.4 mm (1 in.) thick and had a central hole 41.3 mm (1-5/8 in.) in diameter to accommodate the PT bars. These pads were stacked and alternated with 3.2 mm (1/8 in.) thick square steel plates of the same plan dimensions. Each bearing had stiffness equal to 1.46×10^5 kN/m (836 kip/in) when tested at ambient temperature and at a rate varying between 40 and 120 kips/sec. A bearing consisting of four 90 Shore-A hardness polyurethane discs was provided to each post-tensioning bar in test Unit 1B. The discs had a thickness of 47.6 mm (1-7/8 in.), a diameter of 190.5 mm (7.5 in.), and a central hole with a diameter of 47.6 mm (1-7/8 in.) to accommodate the PT bars. The discs stacked and alternated with 190.5 mm (7.5 in.) diameter by 3.2 mm (1/8 in.) thick circular steel plates. Each bearing had stiffness equal to 4.38×10^4 kN/m (250 kip/in) when tested at ambient temperature and at a rate of 0.5 kips/sec.

LOADING PROTOCOL AND TEST RESULTS

Loading Protocol

A vertical force, simulating gravity loads, was applied to the test units by two vertical hollow plunger hydraulic cylinders, positioned above the load stub and connected to the strong floor by one 31.8-mm (1-1/4 in) diameter tie-down rod each (Fig. 3). Actual axial forces of 293 kN (63 kips) and 268 kN (60 kips) were applied to Unit 1A and Unit 1B, respectively. Keeping the gravity force constant, the test unit was subjected to quasi-static reversed cyclic loading by a horizontal actuator in the north-south direction. After three lateral force-controlled cycles to a base shear coefficient of ±0.4 and three to ±0.8, the test proceeded in lateral displacement control. Three cycles to ±0.5% drift ratio and three to ±0.75% were completed. Subsequent cycles consisted of two large-amplitude cycles, followed by a lower one at a level corresponding to the previous large drift level: drift ratios of ±1%, ±1.5%, ±2%, ±3%, ±5%, ±7.5%, and ±10% were targeted.

Figure 7 shows the hysteretic lateral force-displacement response of the two units: lateral displacements have been normalized by the height of the lateral force application point above the column base, and thus, expressed as drift ratios; lateral forces have been normalized by the applied gravity load (equivalent to the weight) and thus transformed into base shear coefficients. For drift ratios larger than 0.3%, it was observed that the base joint rotation was contributing to more than 90% of the lateral displacement: for this reason, drift ratios and joint rotations practically coincided. Figure 8 illustrates the progressive increment of residual drift ratio at the end of each positive cycle, compared to the maximum drift reached during that cycle.

Results for Unit 1A

Testing of Unit 1A resulted in joint opening at the column-mortar bed interface during the cycles to a base shear coefficient of ±0.8; as a consequence a first loss of stiffness was observed on the diagram of Figure 7(*a*). The mortar bed started to flake off during the ±1.5% drift ratio cycles, and showed large flaking off and some visible permanent plastic deformation, without crushing, on the north and south sides (extreme fibers) during the ±3% drift ratio cycles, causing a loss of stiffness. The mortar bed started to crush during the ±5% drift ratio cycles, with significant loss of stiffness and self-centering ability. This corresponds to cycles 25 and 26 in Figure 8(*a*), where residual drift ratios larger than 1.5% can be observed. This was caused by a significant loss of post-tensioning force upon mortar crushing, represented by the decreasing strains bounded by the bottom envelope on Figure 9(*a*).

External dissipators started bending between the buckling-restrained central portion and the end connections during the ±3% drift ratio cycles, due to the rotation imposed by the rocking body motion. The north-west dissipator fractured during the first negative cycle to -7.5% drift ratio, nearly at peak displacement. Two other dissipators fractured on the south side during subsequent cycles. Each fracture corresponded to a jump on the graph of Figure 7(*a*). Due to failure of three out of six dissipators, the test was interrupted after the first cycle to ±10% drift ratio. Residual compressive deformation of the column concrete between the shells, and permanent deformation of the shells themselves due to concrete lateral expansion, was observed at the column base when the column was taken apart from the footing.

The hysteretic stress-strain response of the north-west external dissipator is shown on Figure 9(*b*) up to the first cycle to +5% drift ratio. Strains were measured with a linear potentiometer, connected to the dissipator above and below the milled segment; stresses were calculated from the elastic strains, measured with paired strain gages along the non-disturbed ends of the steel bar. It can be noticed that the peak compressive stresses on the device are larger than the peak tensile ones; this is due to partial composite behavior between the milled bar and the encasing grout and pipe, as the bar non-milled ends bear on the grout.

Results for Unit 1B

Similarly to Unit 1A, joint opening occurred in Unit 1B at the column-mortar bed interface during the cycles to a base shear coefficient of ±0.8; as a consequence a first loss of stiffness was observed on the diagram of Figure 7(*b*). The mortar bed started to flake off during the ±2% drift ratio cycles, and showed large flaking off and some visible permanent compressive deformation, without crushing, on the north and south sides (extreme fibers) during the ±3% drift ratio cycles, causing a loss of stiffness. Mortar bed crushing progressed during the ±5% drift ratio cycles, but not abruptly; it became extensive under the ±7.5% drift ratio cycles, when the stiffness was evidently reduced as well as the self-centering capacity. This corresponds to cycles 28 and 29 in Figure 8(*b*), where residual drifts in the order of 1.5% can be observed.

A first dissipator fractured on the north side during the second negative cycle to -7.5% drift ratio, nearly at peak displacement. A second dissipator fractured on the north side and two on the south side during subsequent cycles. Each fracture corresponded to a jump on the graph of Figure 7(*b*). Residual compressive deformation of the column concrete between the shells, and permanent deformation of the shells themselves due to concrete lateral expansion, was observed at the column base when the column was taken apart from the footing at the end of the test.

Longitudinal and hoop strains were measured close to the base on the outer shell, at the extreme tensile/compressive fibers and in correspondence of two diametrically opposite dissipating dowels. The longitudinal strain profiles measured in front of the south-west dowel, from the base of the shell to the end of the dowel, are plotted in Figure 10. Positive cycles induce tension while negative cycles compression. It can be observed that during cycles up to ±1% drift ratio transfer of tension from the dowel to the shell is distributed within 0.4 times the outer diameter from the base; at larger amplitude cycles it concentrates within 0.2 diameters; above this length, strains remain about constant. Large compressive strains tend to develop close to the base, but no yielding was observed up to ±5% drift ratio cycles.

Comparison between the Responses of Units 1A and 1B

The main difference in the hysteretic response between Units 1A and 1B shows the importance of preventing mortar bed crushing in order to maintain self-centering behavior. Adding polypropylene fibers to the grout mix used in Unit 1B improved the material toughness, thus retarding its crushing and the consequent loss of post-tensioning force. This resulted in recentering capacity extended to cycles to ±5% drift ratio, where Unit 1A was already displaying significant residual displacements, even though larger neutral axis depths were measured on Unit 1B for cycles 7 and beyond compared to Unit 1A (Fig. 11).

CONCLUSIONS

This paper discussed the design criteria and experimental performance of a composite concrete-dual steel shell bridge column technology. These columns can be specifically designed for damage minimization at the design earthquake and to display a self-centering response. The technology simplifies and accelerates bridge construction. The presence of the outer shell make the use of a longitudinal reinforcing cage obsolete, whereas the inner shell remove unnecessary concrete volume, making this technology ideal for prefabrication and easy erection.

Two units were built and tested quasi-statically. The main variables between the two units were: (i) energy dissipation devices, which were either external in the way of buckling-restrained braces or internal in the way of stainless steel dowel bars grouted into the concrete, (ii) the mortar bed, which is required at the column ends to match the surfaces of the adjoining structural elements and also for construction tolerances, and (iii) the type of the elastomeric bearing placed in series with the post-tensioning bars, of either rubber or polyurethane. The units were designed to display no damage at a 3% drift ratio, which was assumed to be the drift ratio corresponding to the design earthquake. Unit 1A, which had a metallic-aggregate mortar bed, showed mortar crushing and compromised self-centering ability during cycles at 5% drift ratio. In Unit 1B the metallic-aggregate mortar bed incorporated also polypropylene fibers. The presence of these fibers delayed the mortar from crushing, allowing this unit to display excellent performance beyond 5% drift ratio. In both units fracture of the energy dissipation devices occurred at drift ratios of 7.5%.

AKCNOWLEDGEMENTS

Funding for this project, provided by the Pacific earthquake Engineering Research Center (PEER) and by the California Department of Transportation (Caltrans), is gratefully acknowledged. The assistance of the technical staff of the Charles Lee Powell Structural Engineering Laboratories at the University of California, San Diego, and the participation of the students G. De Francesco and M. Torres, are duly acknowledged. Discussions with Prof. S. Pampanin and Dr. A. Palermo from the University of Canterbury, New Zealand, were of valuable importance for the development of the external energy dissipators. The authors also thank Salit Specialty Rebars and Hill Brothers Chemical Co. for their support.

REFERENCES

AASHTO (2012). "AASHTO LRFD Bridge Design Specifications, 6th Edition". American Association of State Highway and Transportation Officials, Washington, DC.

ASTM (2010). "Standard Specification for Corrugated Steel Pipe, Metallic-Coated for Sewers and Drains". *ASTM Designation A760/A760M-10,* American Society for Testing and Materials, Philadelphia, PA.

Boyd, P.F., Cofer, W.F., and McLean, D.I. (1995). "Seismic Performance of Steel-Encased Composite Columns under Flexural Loading". *ACI Structural Journal*. **92:3**, 335-364.

Bradford, M.A. (1996). "Design Strength of Slender Concrete-Filled Rectangular Steel Tubes". *ACI Structural Journal*. **93:2**, 229-235.

Caltrans (2010). "Seismic Design Criteria". California Dept. of Transportation, Sacramento, CA.

Christopoulos, C., Filiatrault, A., Uang, C.-M., and Folz, B. (2002). "Post-Tensioned Energy Dissipating Connections for Moment Resisting Steel Frames". *ASCE Journal of Structural Engineering*. **128:9**, 1111-1120.

Cormack, L.G. (1998). "The Design and Construction of the Major Bridges on the Mangaweka Rail Deviation." *Transactions of the Institute of Professional Engineers of New Zealand*. **15**, 6-23.

Culmo, M.P. (2011). "Accelerated Bridge Construction - Experience in Design, Fabrication and Erection of Prefabricated Bridge Elements and Systems". *FHWA Report HIF-12-013*.

El-Sheikh, M.T., Sause, R., Pessiki, S., and Lu, L.-W. (1999). “Seismic Behaviour and Design of Unbonded Post-Tensioned Precast Concrete Frames”. *PCI Journal*, **44:3**, 54-71.

FHWA (2012). http://www.fhwa.dot.gov/bridge/abc/index.cfm

Ge, H. and Usami, T. (1992). “Strength of Concrete-Filled Thin Walled Steel Box Columns: Experiment”. *ASCE Journal of Structural Engineering*. **118:11**, 3036-3054.

Ge, H. and Usami, T. (1994). “Strength Analysis of Concrete Filled Thin Walled Steel Box Columns”. *Journal of Constructional Steel Research*. **37**, 607-612.

Gebman, M., Ashford, S., and Restrepo, J.I. (2006). “Axial Force Transfer Mechanisms within Cast-In-Steel-Shell Piles”. *Report No. SSRP-06/16*, Department of Structural Engineering, University of California at San Diego, La Jolla, CA.

Ghosh, R.S. (1977). “Strengthening of Slender Hollow Steel Columns by Filling with Concrete”. *Canadian Journal of Civil Engineering*. **4:2**, 127-133.

Guerrini, G., and Restrepo, J.I., (2011). “Advanced Precast Concrete Dual-Shell Steel Columns”. *Proceedings of the 8th International Conference on Urban Earthquake Engineering*. **Vol I,** 1125-1129, Tokyo, Japan.

Heiber D.G., (2005). “Precast Concrete Pier Systems for Rapid Construction of Bridges in Seismic Regions”. *Report No. WA-RD 611.1*, Washington Department of Transportation, Olympia, WA.

Hewes, J.T. and Priestley, M.J.N. (2002). **“**Seismic Design and Perfomance of Precast Concrete Segmental Bridge Columns”. *Report No. SSRO-2001/25*, Department of Structural Engineering, University of California at San Diego, La Jolla, CA.

Holden, T., Restrepo, J.I., and Mander, J.B (2003). “Seismic Performance of Precast Reinforced and Prestressed Concrete Walls”. *ASCE Journal of Structural Engineering*. **129:3**, 286-296.

Itani, A.M. (1996). “Future Use of Composite Steel-Concrete Columns in Highway Bridges”. *AISC Engineering Journal*. **33:3**, 110-115.

Karthik, M.M. and Mander, J.B. (2011). “Stress-Block Parameters for Unconfined and Confined Concrete Based on a Unified Stress-Strain Model”. *ASCE Journal of Structural Engineering*. **137:2**, 270-273.

Kato, B. (1996). “Column Curves of Steel-Concrete Composite Members”. *Journal of Constructional*

Steel Research. **39:2**, 121-135.

Kitada, T. (1998). "Ultimate Strength and Ductility of State-of-the-Art Concrete-Filled Steel Bridges Piers in Japan". *Engineering Structures*. **20:4-6**, 347-354.

Knowles, R.B. and Park, R. (1969). "Strength of Concrete Filled Steel Tubular Columns". *ASCE Journal of the Structural Division*. **95:12**, 2565-2587.

Kurama, Y., Sause, R., Pessiki, S., and Lu, L-.W. (1999). "Lateral Load Behavior and Seismic Design of Unbonded Post-Tensioned Precast Concrete Walls". *ACI Structural Journal*, **96:4**, 622-632.

Kwan, W.P. and Billington, S. (2003). "Unbonded Posttensioned Concrete Bridge Piers. I: Monotonic and Cyclic Analyses". *ASCE Journal of Bridge Engineering*, **8:2**, 92-101.

Kwan, W.P. and Billington, S. (2003). "Unbonded Posttensioned Concrete Bridge Piers. II: Seismic Analyses". *ASCE Journal of Bridge Engineering*, **8:2**, 102-111.

Leon, R.T., Kim, D.K., and Hajjar, J.F. (2007). "Limit State Response of Composite Columns and Beam-Columns: Formulation of Design Provisions for the 2005 AISC Specification". *AISC Engineering Journal*, **44:4**, 341-358.

Li, B., Park, R., and Tanaka, H. (1994). "Strength and Ductility of Reinforced Concrete Members and Frames Constructed Using High-Strength Concrete". *Research Report 94-5*, Department of Civil Engineering, University of Canterbury, Christchurch, New Zealand.

MacRae, G.A., and Priestley, M.J.N. (1994). "Precast Post-Tensioned Ungrouted Concrete Beam-Column Subassemblage Tests". *Report No. SSRP-94/10*, Department of Applied Mechanics and Engineering Sciences, University of California at San Diego, La Jolla, CA.

Makris, N. and Roussos, Y. (1998). ''Rocking response and overturning of equipment under horizontal-type pulses''. *Report No. PEER 1998/05*, Pacific Earthquake Engineering Research Center, Berkeley, CA.

Mander, J.B. and Cheng, C.-T. (1997). "Seismic Resistance of Bridge Piers Based on Damage Avoidance Design". *Technical Report NCEER-97-0014*, NCEER, Department of Civil and Environmental Engineering, State University of New York at Buffalo, Buffalo, NY.

Marriott, D., Pampanin, S., and Palermo, A. (2009). "Quasi-Static and Pseudo-Dynamic Testing of Unbonded Post-Tensioned Rocking Bridge Piers with External Replaceable Dissipaters".

Earthquake Engineering and Structural Dynamics. **38**, 331-354.

Marriott, D., Pampanin, S., and Palermo, A. (2011). “Biaxial Testing of Unbonded Post-Tensioned Rocking Bridge Piers with External Replaceable Dissipaters”. *Earthquake Engineering and Structural Dynamics*. **40,** 1723–1741.

Matsui, C., Tsuda, K., and Ishibashi, Y. (1995). “Slender Concrete Filled Steel Tubular Columns under Combined Compression and Bending”. *Proceedings of the 4th Pacific Structural Steel Conference*. **Vol. III,** 29-36, Steel-Concrete Composite Structures.

Nakaki, S.D., Stanton, J. F., and Sritharan, S. (1999). “An Overview of the PRESSS Five-Story Precast Test Building”. *PCI Journal*, **44:2**, 26-39.

Neogi, P.K., Sen, H.K., and Chapman, J.C. (1969). “Concrete-Filled Tubular Steel Columns Under Eccentric Loading”. *The Structural Engineer*. **47:5**, 187-195.

O’Brien, A.D. and Rangan, B.V. (1993). “Tests on Slender Tubular Steel Columns Filled with High-Strength Concrete”. *Australian Civil Engineering Transactions*. **35:4**, 287-292.

O’Shea, M.D. and Bridge, R.Q. (1995). “Circular Thin Walled Concrete Filled Steel Tubes”. *Proceedings of the 4th Pacific Structural Steel Conference*. **Vol. III,** 53-60, Steel-Concrete Composite Structures.

Ou, Y.-C., Chiewanichakorn, M., Ahn, I.-S., Aref, A.J., Chen, S.S., Filiatrault, A., and Lee, G.C. (2006). “Cyclic Performance of Precast Concrete Segmental Bridge Columns: Simplified Analytical and Finite Element Studies”. *Transportation Research Record: Journal of the Transportation Research Board*. **1976**, 66-74.

Ou, Y.-C., Wang, P.-H., Tsai, M.-S., Chang, K.-C., and Lee, G.C. (2010). “Large-Scale Experimental Study of Precast Segmental Unbonded Posttensioned Concrete Bridge Columns for Seismic Regions”. *ASCE Journal of Structural Engineering*. **136:3**, 255-264.

Palermo, A. and Pampanin, S. (2008). “Enhanced Seismic Performance of Hybrid Bridge Systems: Comparison with Traditional Monolithic Solutions”. *Journal of Earthquake Engineering*. **12:8**, 1267-1295.

Palermo, A., Pampanin, S., and Calvi, G.M. (2005). “Concept and Development of Hybrid Solutions for Seismic Resistant Bridge Systems”. *Journal of Earthquake Engineering*. **9:6**, 899-921.

Palermo, A., Pampanin, S., and Marriott, D. (2007). "Design, Modeling, and Experimental Response of Seismic Resistant Bridge Piers with Posttensioned Dissipating Connections". *ASCE Journal of Structural Engineering*. **133:11**, 1648-1661.

Park, RJT and Paulay, T. (1990). "Strength and Ductility of Concrete Substructures of Bridges". *Transit New Zealand - Road Research Unit Bulletin*. **84:1**, 14-29.

Park, RJT, Priestley, MJN, and Walpole, WR. (1983). "The Seismic Performance of Steel Encased Reinforced Concrete Bridge Piles". *Bulletin of the New Zealand National Society for Earthquake Engineering*. **16:2**, 123-140.

Paulay, T. and Priestley, M.J.N. (1992). *Seismic Design of Reinforced Concrete and Masonry Buildings*. John Wiley and Sons, New York, NY.

Pérez, F.J., Pessiki, S., Sause, R., and Lu, L.-W. (2003). "Lateral Load Tests of Unbonded Post-Tensioned Precast Concrete Walls". *Special Publication of Large-Scale Structural Testing, Paper No. SP 211-8*, American Concrete Institute, Detroit, 161-182.

Priestley, M.J.N., Sritharan, S., Conley, J.R., and Pampanin, S. (1999). "Preliminary Results and Conclusions from the PRESSS Five-Story Precast Concrete Test Building". *PCI Journal*, **44:6**, 42-67.

Priestley, M.J.N., and Tao, J.R.T. (1993). "Seismic Response of Precast Prestressed Concrete Frames with Partially Debonded Tendons". *PCI Journal.* **38:1**, 58-69.

Prion, H.G.L. and Boehme J. (1989). "Beam-Column Behaviour of Steel Tubes Filled with High-Strength Concrete". *Fourth International Colloquium*, SSRC, New York, 439-449.

Rangan, B.V. and Joyce, M. (1992). "Strength of Eccentrically Loaded Slender Steel Tubular Columns Filled with High Strength Concrete". *ACI Structural Journal*. **89:6**, 676-681.

Restrepo, J.I. and Rahman, A. (2007). "Seismic Performance of Self-Centering Structural Walls Incorporating Energy Dissipators". *ASCE Journal of Structural Engineering*. **133:11**, 1560-1570.

Restrepo, J.I., Tobolski, M.J., and Matsumoto, E.E. (2011). "Development of a Precast Bent Cap System for Seismic Regions". *NCHRP Report 681*.

Sakai, J. and Mahin, S.A. (2004). "Analytical Investigations of New Methods for Reducing Residual Displacements of Reinforced Concrete Bridge Columns". *Report No. PEER 2004/02*, Pacific

Earthquake Enigneering Research Center, Berkeley, CA.

Sakai, J., Jeong, H., and Mahin, S.A. (2006). “Reinforced Concrete Bridge Columns that Recenter Following Earthquakes”. *Proceedings of the 8th U.S. National Conference on Earthquake Engineering*, Paper No. 1421, San Francisco, CA.

Sakino, K. and Ishibashi, H. (1985). “Experimental Studies on Concrete Filled Square Steel Tubular Short Columns subjected to Cyclic Shearing Force and Constant Axial Force”. *Transactions, Architectural Institute of Japan*. **353(July)**, 81-89, Tokyo, Japan.

Sakino, K. and Tomii, M. (1981). “Hysteretic Behaviour of Concrete Filled Square Shell Tubular Beam-Columns Failed in Flexure”. *Transactions, Japan Concrete Institute*. **3**, 439-446, Tokyo, Japan.

Shakir-Khalil, H. and Zeghiche, J. (1989). “Experimental Behaviour of Concrete-Filled Rolled Rectangular Hollow Section Columns”. *The Structural Engineer*. **67:19**, 346-353.

Shakir-Khalil, H. and Mouli, M. (1990). “Further Tests on Concrete-Filled Rectangular Hollow Section Columns”. *The Structural Engineer*. **68:20**, 405-413.

Shanmugam, N.E. and Lakshmi, B. (2001). “State of the Art Report on Steel-Concrete Composite Columns”. *Journal of Constructional Steel Research*. **57**, 1041-1080.

Sharpe, R.D. and Skinner, R.I. (1983). “The Seismic Design of an Industrial Chimney with Rocking Base”. *Bulletin of the New Zealand National Society for Earthquake Engineering*, **16:2**, 98-106.

Solberg, K. Mashiko, N., Mander, J.B., and Dhakal, R.P. (2009). “Performance of a Damage-Protected Highway Bridge Pier Subjected to Bidirectional Earthquake Attack”. *ASCE Journal of Structural Engineering*. **135:5**, 469-478.

Stone, W.C., Cheok, G.S., and Stanton, J.F. (1995). “Performance of Hybrid Moment-Resisting Precast Beam-Column Concrete Connections Subjected to Cyclic Loading”. *ACI Structural Journal*. **91:2**, 229-249.

Suzuki, H. and Kato, B. (1981). “Shear Strength of Concrete Filled Box Elements”. *Proceedings of the Conference on Joints in Structural Steelwork*, Middlesborough, England.

Toranzo, L.A., Restrepo, J.I., Mander, J.B., and Carr, A.J. (2009). “Shake-Table Tests of Confined-Masonry Rocking Walls with Supplementary Hysteretic Damping”. *Journal of Earthquake*

Engineering. **13:6**, 882-898.

Uy, B. and Patil, S.B. (1996). "Concrete-Filled High Strength Steel Box Columns for Tall Buildings: Behaviour and Design". *The Structural Design of Tall Buildings*. **5**, 75-93.

Virdi, K.S. and Dowling, P.J. (1973). "The Ultimate Strength of Composite Columns in Biaxial Bending". *Proceedings of the Institution of Civil Engineers, Part 2*. **55(Mar.)**, 251-272.

Wang, Y.C. and Moore, D.B. (1997). "A Design Method for Concrete-Filled Hollow Section Composite Columns". *The Structural Engineer*. **75:21**, 368-372.

FIGURES AND TABLES

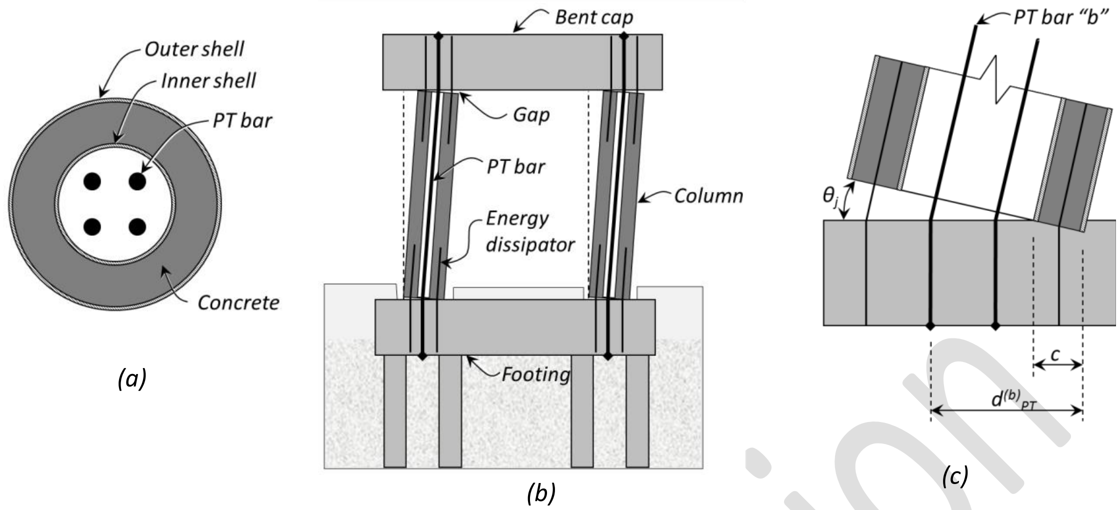

Figure 1. Sketches of the proposed system: (a) column typical cross-section; (b) bent components and rocking kinematics; (c) joint rotation.

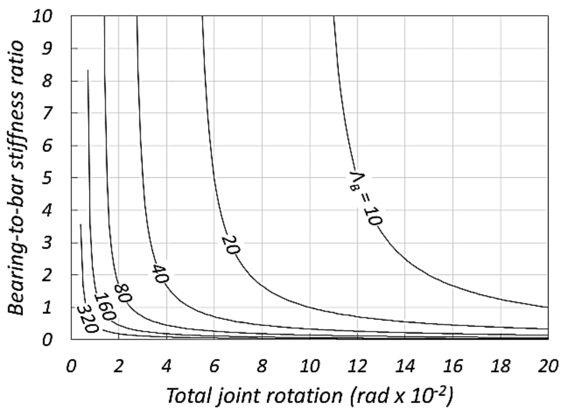

Figure 2. Design chart for deformable devices (bearings) in series with post-tensioning bars.

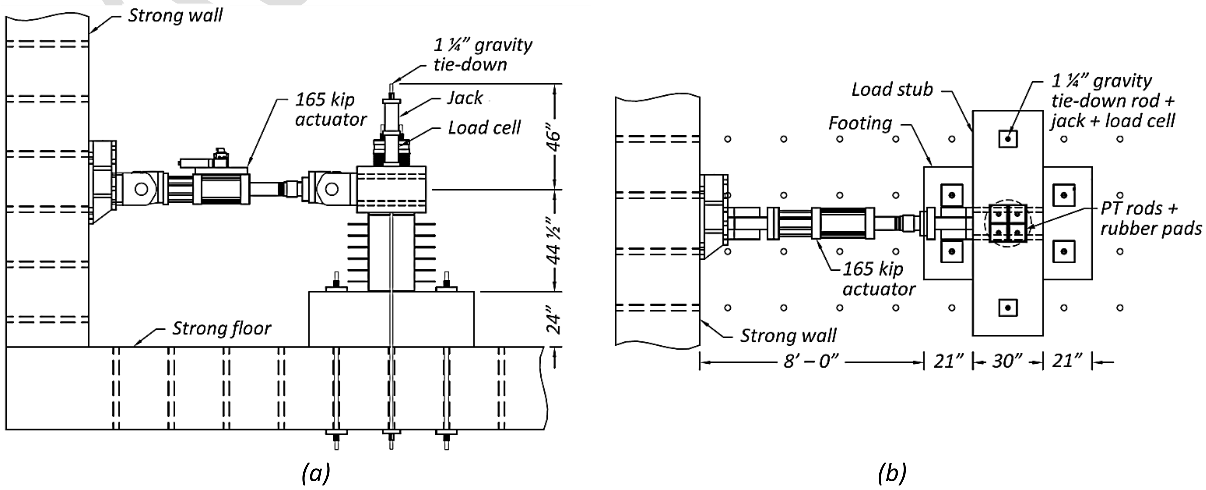

Figure 3. Test setup and dimensions: (a) side view; (b) top view.

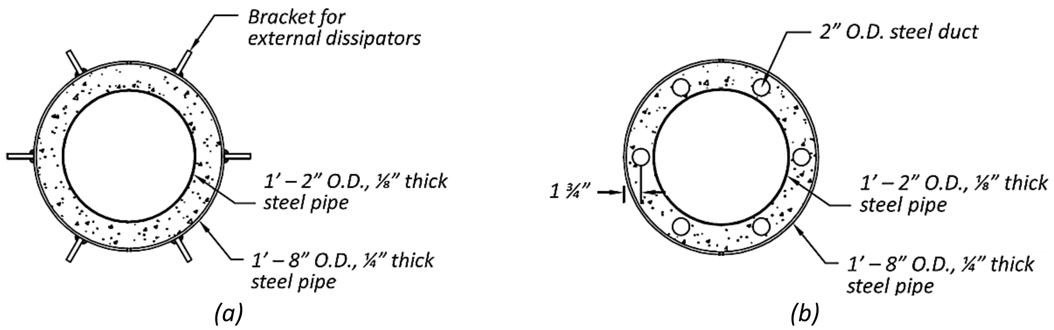

Figure 4. Column base cross-sections: (a) Unit 1A; (b) Unit 1B.

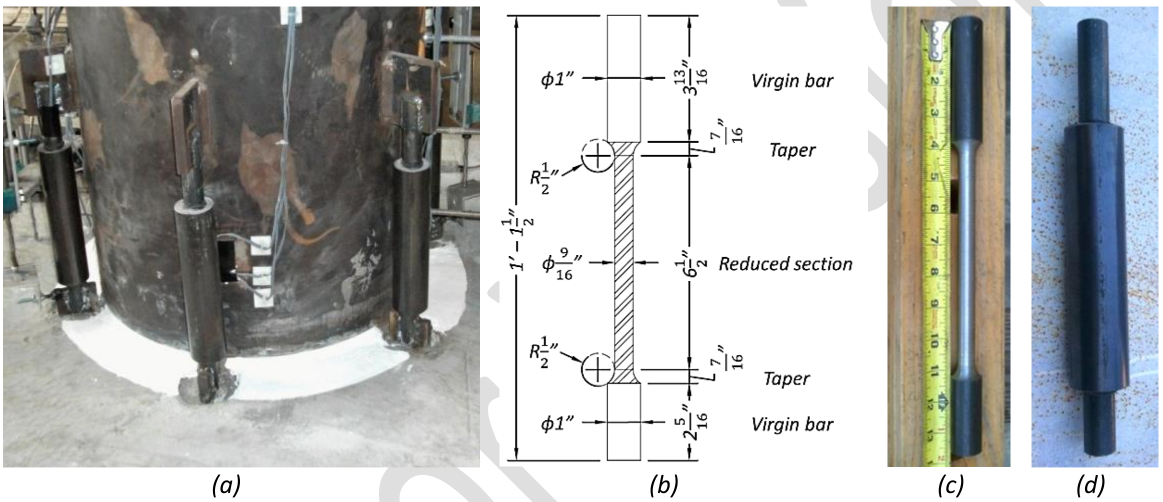

Figure 5. External energy dissipators: (a) location around column perimeter; (b) construction details; (c) dog-bone milled steel bar; (d) assembled buckling-restrained device.

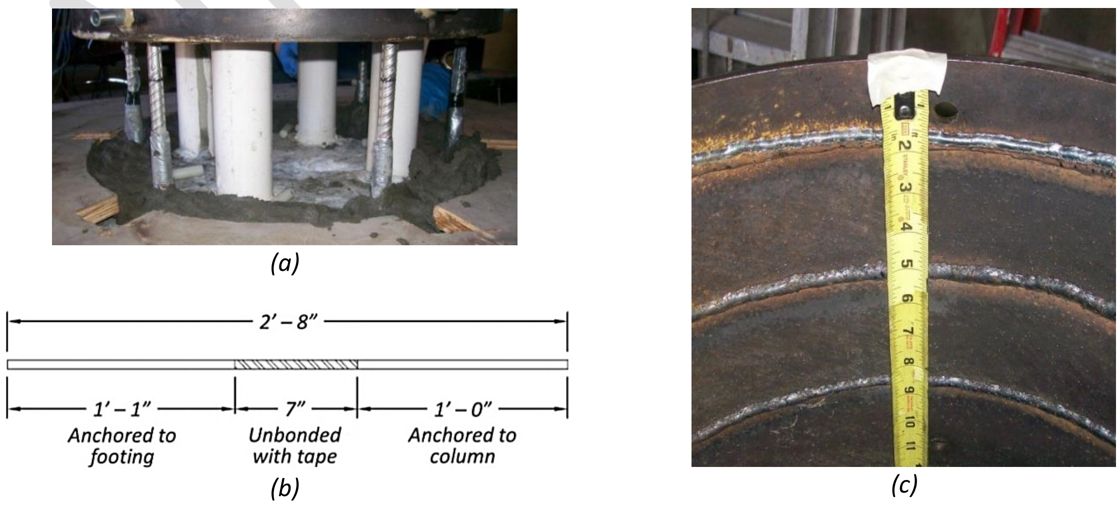

Figure 6. Internal energy dissipators: (a) dowels during column placement; (b) construction details; (c) circumferential weld beads on the interior surface of the outer shell.

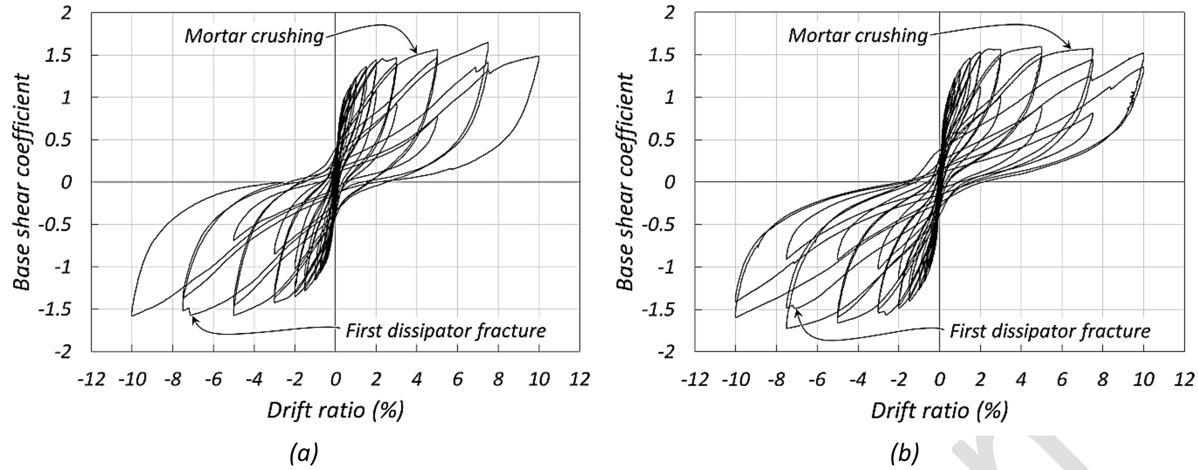

Figure 7. Hysteretic lateral force-displacement response: (a) Unit 1A; (b) Unit 1B.

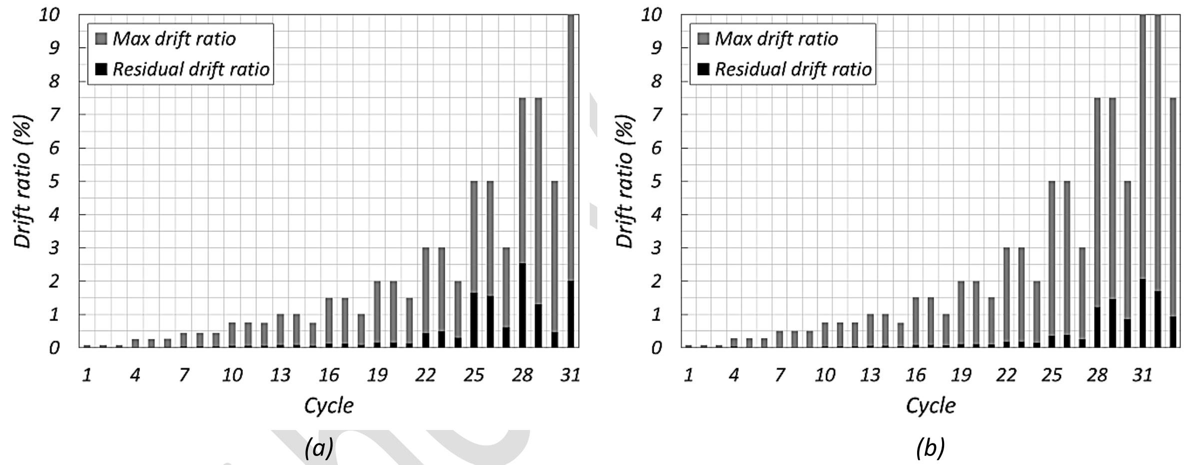

Figure 8. Maximum (grey) and residual (black) drift ratios. Only cycles to positive displacements are reported: (a) Unit 1A; (b) Unit 1B.

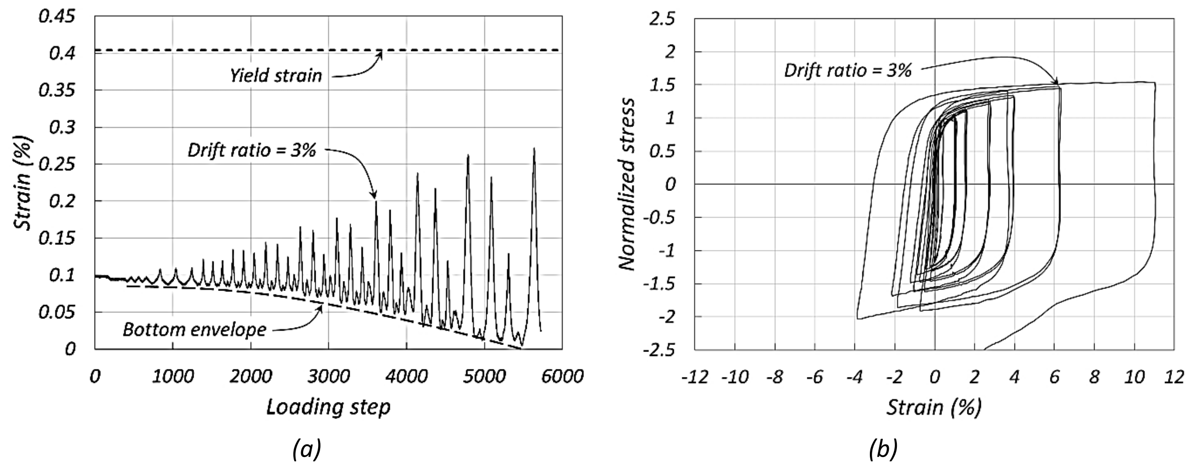

Figure 9. Response of Unit 1A: (a) north-east post-tensioning bar strain history; (b) north-west energy dissipator hysteretic loops.

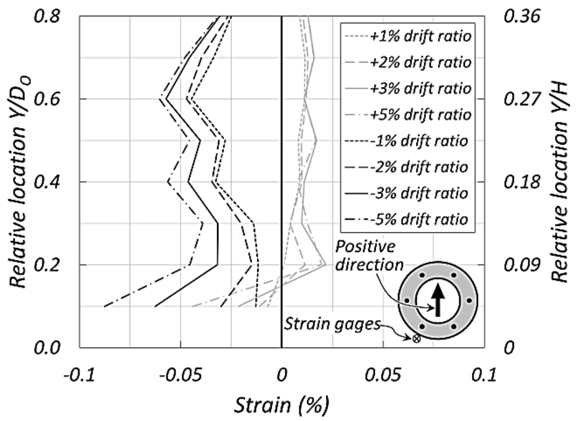

Figure 10. Outer-shell longitudinal strain profiles in correspondence of the south-west dowel for Unit 1B.

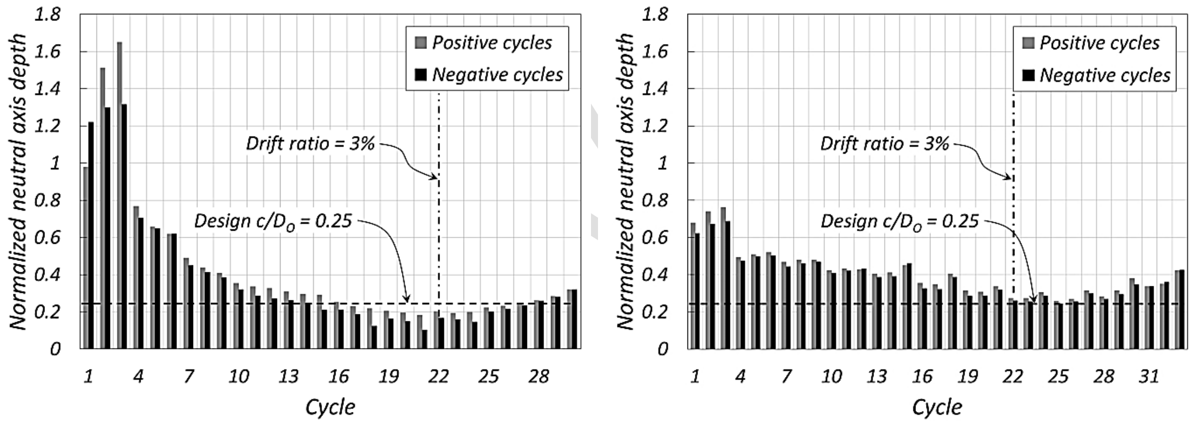

(a) (b)

Figure 11. Experimental neutral axis depth at peak lateral displacements: (a) Unit 1A; (b) Unit 1B.